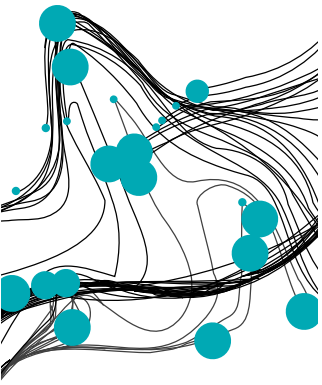

RAM ROBOTICS AND MECHATRONICS

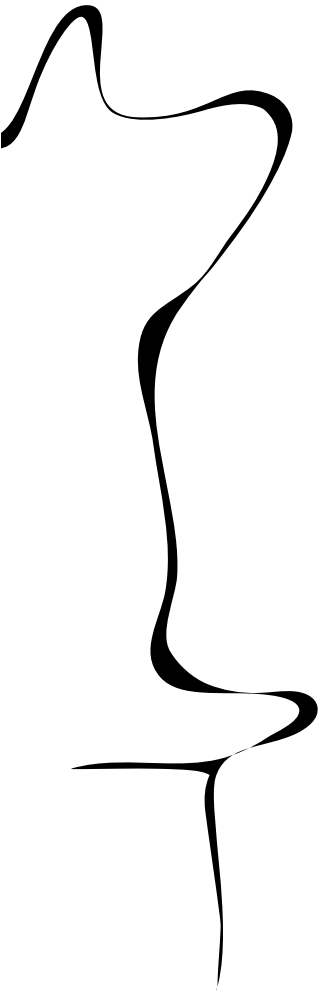

TENDON ROUTING OPTIMIZATION OF A TENDON-DRIVEN GRIPPER TO REDUCE FRICTIONAL EFFECTS

B.A.J. (Boris) Feldbrugge

BSC ASSIGNMENT

Committee:
B. Okken
dr. ir. W. Roozing
dr. ir. J.J. de Jong

february, 2024

004RaM2024
Robotics and Mechatronics
EEMCS
University of Twente
P.O. Box 217
7500 AE Enschede
The Netherlands

UNIVERSITY OF TWENTE. | TECHMED CENTRE
UNIVERSITY OF TWENTE. | DIGITAL SOCIETY INSTITUTE

Tendon routing optimisation of a tendon-driven gripper to reduce frictional effects

Boris Feldbrugge, Electrical Engineering UTwente, dept. RaM

***Abstract*—We present a tendon routing optimisation method for reducing the static friction experienced in a tendon-driven mechanism. Tendon-driven mechanisms enable the designer to have the actuator placed away from the actuated joint, where the tendons give the opportunity for a slim design. One of the drawbacks of a tendon-driven mechanism is a relatively poor force transmission efficiency between the actuator and the joint(s) due to frictional effects. To optimise the force transmission efficiency we will develop a static friction model of a tendon-driven mechanism. We then propose, with the developed model, a design optimisation method to reduce static frictional effects. A variety of tests demonstrate the performance and the viability of this optimisation applied to the tendon routing of an existing tendon-driven gripper.**

I. Introduction

The agro and food industry currently faces the challenge, due to our large population, of having to supply to a high demand for food but lacking the space to expand to. One of the solutions is the use of robots due to their ability to work continuously, however the application of robots come with it's own sets of challenges.

Grasping and manipulation of objects is a recurring challenge in robotic gripper design. Grippers need to adapt to variations in the object's size, surface finish, and shape. While the object should remain undamaged at the same time. Next to object manipulation other relevant requirements include build cost and gripper size.

One of the possible approaches to deal with object variation, is using variable stiffness and under-actuation. Mart Bluiminck et al. present a two fingered tendon-driven gripper[1] design using these principles, for the use in the agro-food industry. The gripper features a symmetrical, dual-phalanx design and the gripper is designed to execute a pinch grasp and enveloping grasp on a certain range of objects. The actuation of the gripper is through a tendon-driven mechanism which enables the actuators to be placed outside of the gripper. A drawback of tendon-driven mechanisms, which is also evident from the measured results of the prototype[1], is the friction it can introduce to the actuation system. A tendon requires routing points as they help to keep the tendon routing continuous during the stroke. These routing points play a major role in the friction experienced by the tendon, which is undesirable for multiple reasons. Firstly the friction deteriorates the force transmission efficiency(FTE), secondly position control is negatively affected by the friction due to the stick-slip effect[2]. Another undesired side effect of friction is that it causes wear in the mechanism.

Some works have investigated optimal design of routing points for tendon-driven mechanisms. Dong et al. [3] introduce an optimisation of a design with special emphasis on reducing friction. Although the derivation of the contact forces and workspace are applicable, due to the three phalanx design and different routing topology the friction model cannot be applied to the previous work[1]. Additionally, the friction model used by Dong et al. neglects the radii of the routing points in the mechanism which will have an influence on the optimised result.

The main contribution of this work is a model describing static frictional effects of a tendon-driven gripper that takes the radii of the routing points in account, which is subsequently optimised to reduce frictional effects. We will describe the friction of previous work[1] as a reference. The design will be optimised and the optimisation is evaluated by comparing it's force transmission efficiency compared to previous work[1].

The paper is structured as follows: Sec. II covers the model describing the friction in a tendon-driven mechanism. This model is then used to optimise one tendon route that's part of an existing tendon-driven mechanism in Sec. III. Followed by the results of this optimisation in Sec. IV. Next, Sec. V and Sec. VI will discuss the results/method of optimisation and conclude if the proposed method does improve the force transmission efficiency of a tendon routing design. At last will Appendix A and Appendix A feature supplementary information.

II. Model

An optimisation requires a sufficiently accurate model to succeed. This model consists of an expression for the static friction in the system and the formulation for the continuity of the tendon's contact with the pulleys during the stroke. This section will go in more detail on the current gripper design[1] and the decisions made for the model in this research.

A. Gripper geometric model

Exact dimensions and the range of the joint angles of the current gripper, which is displayed in Fig. 1, are in Appendix A.

The configuration of the mechanism is expressed in the body fixed frames per link, which simplifies the expression of the model. We use homogeneous transformation matrices to convert the placement of all components to a fixed space frame, which is placed in the middle of the base of the gripper Fig. 1. Frame B is situated at the center of pulley one and frame C is in the center of pulley two. The angle 'θ_1' is the angle that link one makes with the base link and has a counter clockwise direction. Angle 'θ_2' is the angle that link two makes around the center of the second pulley and has

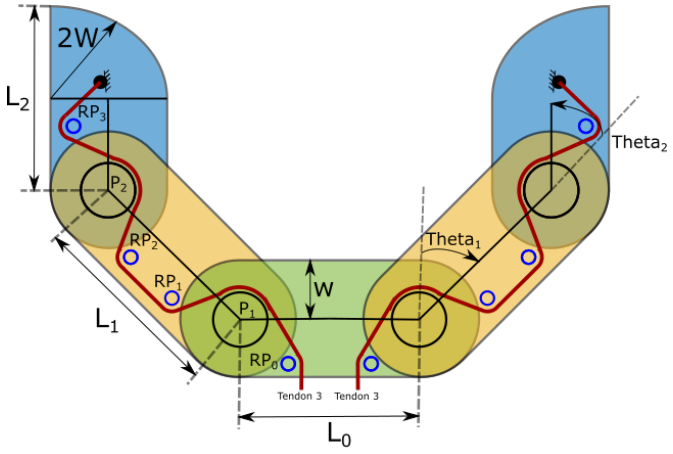

Fig. 1. The tendon routing through one finger of the gripper.

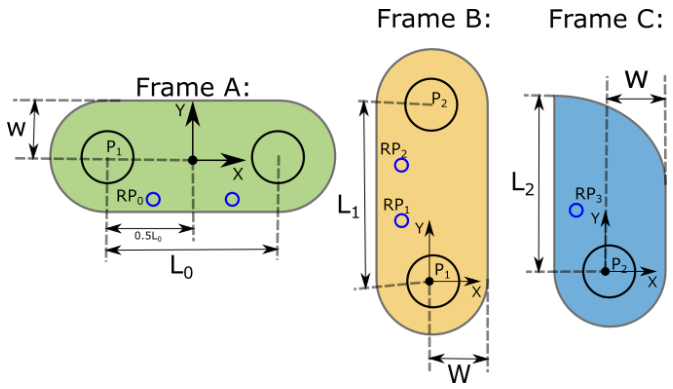

Fig. 2. The three kinematic frames next to each other

a clockwise direction.Eq. (1), Eq. (2) and Eq. (3) show the associated homogeneous transformations between the frames.

$$H_B^A = \begin{bmatrix} cos(\theta_1) & -sin(\theta_1) & {}^A x_B \\ sin(\theta_1) & cos(\theta_1) & {}^A y_B \\ 0 & 0 & 1 \end{bmatrix} \tag{1}$$

$$H_C^B = \begin{bmatrix} cos(-\theta_2) & -sin(-\theta_2) & {}^B x_C \\ sin(-\theta_2) & cos(-\theta_2) & {}^B y_C \\ 0 & 0 & 1 \end{bmatrix} \tag{2}$$

$$H_C^A = H_B^A * H_C^B \tag{3}$$

As can be seen from Fig. 1 the two fingers feature an identical, but mirrored configuration. Additionally all three tendons in both fingers are coupled to their counterpart through a differential pulley system. The differential pulley system is to account for object irregularities or misalignment of the object. Due to the similarity of the fingers, the analysis/model of this research will cover only one finger. This will simplify the model. We will focus on the optimisation of the third tendon in the gripper. This tendon is chosen because it features the most amount of tendon contact points, consisting of four routing points and both pulleys, and it will proof the concept of this optimisation method sufficiently.

1) Wrapping angle calculation: The wrapping angle is needed for calculating the force transmission efficiency for both the routing points and the pulleys, as will be explained in Sec. II-B. The tendon will be treated as a tangent line between each routing point/pulley and with it we can calculate the wrapping angles per routing points/pulleys through a multi-step procedure. Firstly we determine which tangent lines correspond with the tendon route, secondly we map every routing point and pulley to base frame coordinates (kinematic frame A), thirdly we calculate the entry and leave points based on the tendon route and at last we calculate the wrapping angle per routing point and pulley based on their entry and departure point. Now we will follow this procedure in more detail.
First we determine the tangent lines, which also determines the tangent points, according to the tendon route of the mechanism. There are four type of tangent lines, inner tangent lines between two circles, outer tangent lines between two different sized circles, outer tangent lines for two circles with the same radius and the tangent line between a point and a circle

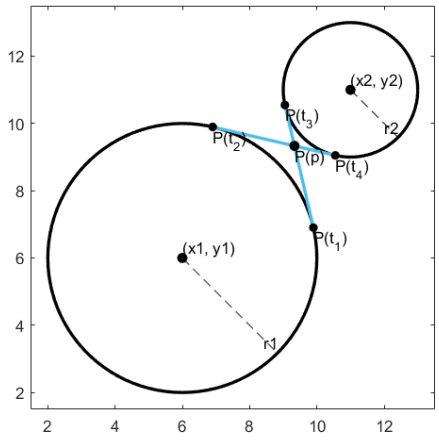

Fig. 3. Two circles of different sizes with their inner tangent lines. indicated coordinates: centers of both circles, tangent points on circles (numbered), tangent point P.

We need for the inner tangent points of two circles, as in Fig. 3, their center coordinates (x_{C1},y_{C1}) and (x_{C2},y_{C2}) and their radii (r1 and r2) to derive the point 'P'. Point 'P' is the point where the two inner tangent lines cross each other, it's expression is given in Eq. (4).

$$\begin{aligned} x_p &= \frac{x_2 r_1 + x_1 r_2}{r_1 + r_2} \\ y_p &= \frac{y_2 r_1 + y_1 r_2}{r_1 + r_2} \end{aligned} \tag{4}$$

Coordinates for the tangent points on circle 1:

$$x_{t_{1,2}} = \frac{r_0^2(x_p - x_1) \pm r_1(y_p - y_1)\sqrt{(x_p - x_1)^2 + (y_p - y_1)^2 - r_1^2}}{(x_p - x_1)^2 + (y_p - y_1)^2} + x_1$$
$$y_{t_{1,2}} = \frac{r_1^2(y_p - y_1) \mp r_1(x_p - x_1)\sqrt{(x_p - x_1)^2 + (y_p - y_1)^2 - r_1^2)}}{(x_p - x_1)^2 + (y_p - y_1)^2} + y_1 \quad (5)$$

Coordinates for the tangent points on circle 2:

$$x_{t_{3,4}} = \frac{r_1^2(x_p - x_2) \pm r_1(y_p - y_2)\sqrt{(x_p - x_2)^2 + (y_p - y_2)^2 - r_2^2}}{(x_p - x_2)^2 + (y_p - y_2)^2} + x_2$$
$$y_{t_{3,4}} = \frac{r_2^2(y_p - y_2) \mp r_2(x_p - x_2)\sqrt{(x_p - x_2)^2 + (y_p - y_2)^2 - r_2^2)}}{(x_p - x_2)^2 + (y_p - y_2)^2} + y_2 \quad (6)$$

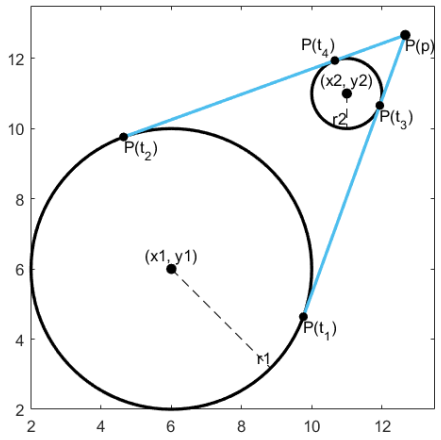

Fig. 4. Two different sized circles with the outer tangent lines, indicated coordinates: centers of both circles, tangent points on circles, point P.

The calculation of the outer tangent points of two different sized circles has the same definitions for the tangent points as the inner tangent points. The only change are the coordinates for the point P, which is calculated in Eq. (7).

$$x_p = \frac{x_2 r_1 - x_1 r_2}{r_1 - r_2}$$
$$y_p = \frac{y_2 r_1 - y_1 r_2}{r_1 - r_2} \quad (7)$$

The outer tangent points of two circles of the same size are the points on the circle where the line crosses that is perpendicular to the vector between the center of the two circles. The tendon in this model starts in the entry point and is routed to the first routing point. We assume that the tendon will enter at the right most point of the first routing point, so it enters this routing point at zero radians compared to base frame A. This is assumed since the situation of how the tendon enters the gripper will not be assessed by this research.

As both the entry and leave coordinates are now known, we can derive their wrapping angle as follows:
we first place the origin in the center of the circle in question, then we retrieve the angle (θ_E) in the polar coordinates that the entry point makes with the frame of the center of the circle. We wrap this angle to the range of 0π to 2π. We retrieve the departure point expressed in the entry frame by multiplying the coordinates in center frame with the rotation matrix from center to entry frame:

$$R_{Center}^{Entry} = \begin{bmatrix} cos(\theta_E) & -sin(\theta_E) \\ sin(\theta_E) & cos(\theta_E) \end{bmatrix}$$
$${}^{Entry}P_{Depart} = R_{Center}^{Entry} * {}^{O}P_{Depart} \quad (8)$$

These coordinates are then used to calculate the angle between the entry and departure points, this angle will again be wrapped to a range of 0 to 2pi to prevent zero crossings when the tendon wraps around a routing point/pulley for more than pi radians. According to if the tendon goes anticlockwise or clockwise the result is the angle θ or $2\pi - \theta$.

B. Friction model

The friction for this optimisation will only be described by the static friction introduced by the tendon touching the routing points and pulleys. The reason for this simplification is because we are interested in the contact forces between the gripper and the object, and hence both are in a static situation.
We assume, according to [4], that the FTE relations of the pulleys and the routing points are different from each other. This is because the tendon slips over the routing points and doesn't slip over the pulleys because they are bushing supported. We assume that the routing points, until the phalanx where the tendon is attached to, affect the total force transmission efficiency for the tendon of interest. The routing points between the attachment point and the pulley at the beginning of that phalanx do not affect the transmission efficiency. That is because there is no relative movement of the tendon over this routing point, it does affect the position where the tendon leaves the earlier mentioned pulley.

1) Routing point friction: The friction over static routing points can be approximated by slip friction and the capstan equation. Peng et. al. [4] present an equation to evaluate force transmission efficiency of the routing points, which is shown in Eq. (9). Where μ is the friction coefficient between the routing point material and the material that slips over it. The 'θ' represents the wrapping angle around the routing point.

$$\eta_{RP} = e^{-\mu * \theta} \quad (9)$$

The tendon used in the prototype of previous work [1] is made from polyethylene [5] and the routing points are metal pins, so the μ of used in this friction model between the tendon and routing points is approximated to be 0.2 [6].

2) Pulley Friction: The pulleys are, contrary to the routing points, bushing supported. Which means that there is no relative movement between the tendon and the pulley thus the force transmission efficiency of the pulleys is determined differently. Peng et. al. [4] present an equation to evaluate the force transmission efficiency for bushing supported pulleys, which is shown in Eq. (11). The friction is based on the normal force acting on the journal of the bearing, which is dependent on the tension force of the tendon before (T_1) and after (T_2) the pulley. With the relation '$T_2 = \eta T_1$' we can eliminate

the terms of the tension forces in the relation of the FTE of a bushing supported pulley. The force transmission efficiency Eq. (11) is based around the angle that the tendons make with each other (Eq. (10), the mu of the bushing, inner diameter of bushing 'r_j'(since we assume that the bushing is mounted on the pulley) and pulley radius 'r_p'. We choose as the bushing's μ the value 0.08, this is the iglidur G type bushing under high load[7].

$$\theta_t = \pi - \theta_{wrapPulley} \tag{10}$$

$$\begin{aligned} \alpha &= \frac{r_p}{r_j * \mu_{bushing}} \\ \eta_P &= \frac{\alpha^2 + cos(\theta_t) - \sqrt{(1 + cos(\theta_t))(2\alpha^2 + cos(\theta_t) - 1)}}{\alpha^2 - 1} \end{aligned} \tag{11}$$

III. Optimisation

The presented model can be used in combination with computational optimisation in order to reduce friction in the mechanism. First we setup the optimisation method, followed by declaring the optimisation boundaries and the cost function of the optimisation.
As optimisation method we will use a local optimiser method that starts at an initial guess and minimises a function based on it's gradient inside the given constraints.

A. Optimisation cost function

The cost function is shown in Eq. (12).

$$\begin{aligned} \eta_{tendon} &= \eta_{RP0}\eta_{RP1}\eta_{RP2}\eta_{RP3}\eta_{P1}\eta_{P2} \\ \mathcal{F}(p) &= \frac{1}{\eta_{Tendon}} + \alpha * \sum (e^{-\gamma D_{contact}}) \end{aligned} \tag{12}$$

The cost function has as input the body fixed frame coordinates of each routing point. The reason for the body fixed frame coordinates is to make formulating boundaries easier. The cost function optimises the position of the routing points for the given combination of the angles of both phalanges while maintaining contact with the pulleys in the two extremes of the two joint angles due to a soft constraint. We assume that the FTE will be improved over the whole range of joint angle configurations of the mechanism by this method of optimising. To maximise the force transmission efficiency the cost function consists of the inverse of this efficiency since the optimisation method minimises the outcome of the cost function.

In order to guarantee contact between the tendons and pulleys, soft constraints have been added to the cost function. The distance between the entry point of the pulley and the next routing point should be greater than the distance between the departure point of the pulley and the next routing point when the tendon touches the pulley.

The cost function also features a soft constraint for both pulleys to preserve the tendon touching the pulleys. The soft constraint is a function of a 'constant stroke' parameter ($D_{contact}$) which will be elaborated on in Sec. III-A1. The soft constraint is an inverse exponential to retain the continuity of the cost function. it's value is close to zero when $D_{contact}$ is positive and it's value will increase with a certain gradient when $D_{contact}$ becomes negative. Gain 'γ' increases the gradient of the soft constraint. The main effect of parameter 'α' is to attenuate the soft constraint for when $D_{contact}$ is non negative.
In total there are four soft constraints, one for the minimum and maximum angle of both joints.

1) Constant stroke soft constraint ($D_c$ontact): Dong et.al.[3] assume the moment arm of the joint to be the pulley radius, if and only if the tendon is touching the pulley. This property is important to preserve during the optimisation because a continuous function of the force that the gripper is applying would simplify the controls of the gripper.
Ideally we have a continuous function describing the contact between the pulley and the tendon. Which is possible if we make an assumption that the wrapping angle of the pulley will stay in the range of zero to $\frac{\pi}{2}$ radians. This would mean that the distance between the center of the next routing point and the entry point of this pulley would be greater than the distance between that same center and the departure point of this pulley. Subtracting both distances from each other respectively would result in a 'contact distance' that is positive if the tendon would touch the pulley, and a negative 'contact distance' if the tendon wouldn't touch the pulley.

B. Optimisation boundaries

The boundaries set to the optimisation are to prevent results with routing points placed outside of the gripper. The boundaries for this optimisation are given in Sec. III-B. Where most of the boundaries are to prevent collision with the pulleys and placement outside of the phalanxes there is one exception. The exception lays in the boundaries of routing points one and two, since they are located on the same phalanx. Due to the method of calculating the wrapping angles it is necessary to maintain the routing points in the same sequence during the optimisation. This is done by restricting the possible locations of both routing points one and two to the half of the phalanx closest to their respective pulley.

Parameter	Lower bound	Upper bound
x_{RP0} w.r.t. frame A	$-0.5 * L_0 + r_{P1} + r_{RP0}$	0
y_{RP0} w.r.t. frame A	$-W$	$w - r_{RP0}$
x_{RP1} w.r.t. frame B	$-W + r_{RP1}$	$W - r_{RP1}$
y_{RP1} w.r.t. frame B	$r_{P1} + r_{RP1}$	$0.5 * L_1 - r_{RP1}$
x_{RP2} w.r.t. frame B	$-W + r_{RP2}$	$W - r_{RP2}$
y_{RP2} w.r.t. frame B	$0.5 * L_1 + r_{RP2}$	$L_1 - r_{P2} - r_{RP2}$
x_{RP3} w.r.t. frame C	$-W + r_{RP3}$	$W - r_{RP3}$
y_{RP3} w.r.t. frame C	$r_{P2} + r_{RP3}$	$L_2 - r_{RP3} - 2W$

IV. Results

The optimised tendon routing can be seen in Fig. 5. The optimised routing point positions can be seen in Appendix A. The FTE of the original design with both joints being folded $\frac{\pi}{4}$ radians in this friction model is 0.6314. Whereas the FTE of the optimised design in the same configuration is 0.7906,

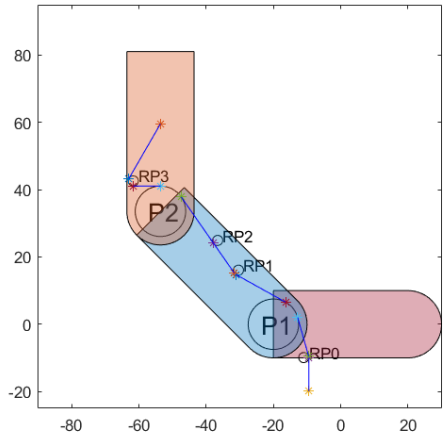

Fig. 5. The optimised tendon routing visualised in the gripper mechanism

which is an improvement of 25%. These results are with the four soft constraints having a 'γ' of 1000 and an 'α' of 0,01.

The output of the cost function per iteration in Fig. 6 shows the development of the optimisation process for the given parameters.

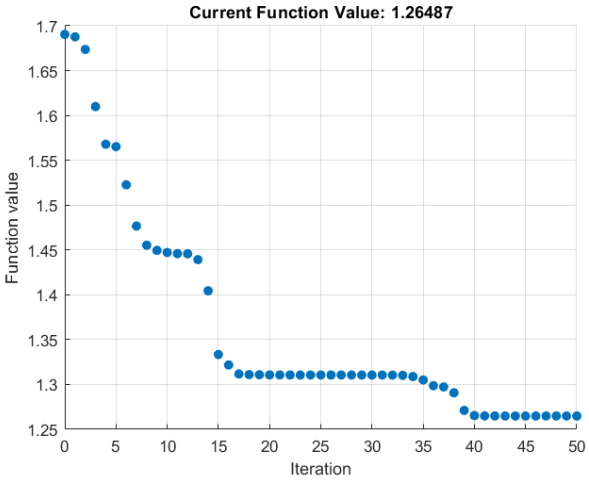

Fig. 6. The output of the cost function $\mathcal{F}(p)$ over the iterations.

The surface plots in Fig. 7 and Fig. 8 show the FTE of the mechanism over a range of joint angle configurations. The initial design features the lowest FTE at the most folded position of 0,61. The highest FTE of the initial design is at the configuration where both joints are unfolded the most with an efficiency of 0,65. The optimised result features a similar trend of efficiency over the range of configurations, but with the outer values of efficiency being 0,76 and 0,79 respectively.

V. Discussion

The results of the optimisation method are discussed and summarised in this section in a few points below.

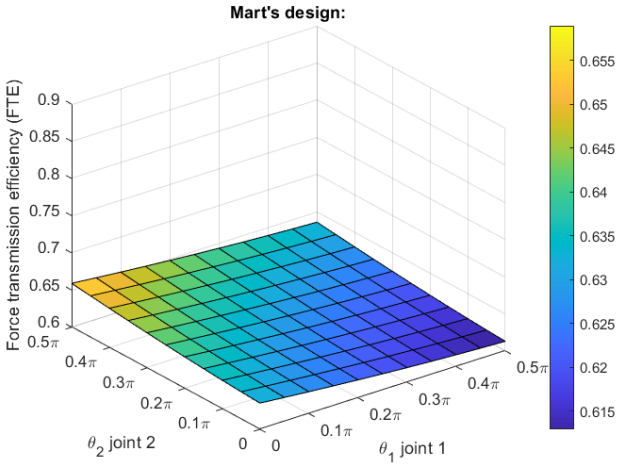

Fig. 7. The force transmission efficiency over multiple joint angle configurations of the original design. The lowest efficiency is at the configuration where the finger is stretched ($\eta = 0.61$). The tendon has the highest efficiency when the finger is folded ($\eta = 0.66$).

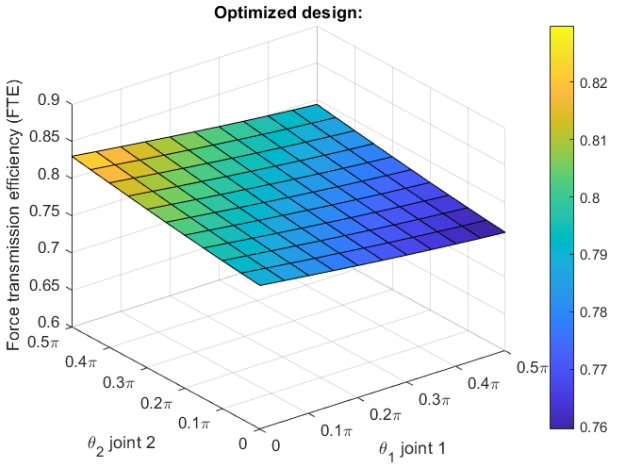

Fig. 8. The force transmission efficiency over multiple joint angle configurations of the optimised (insert for which configuration it was optimised) design.The lowest efficiency is at the configuration where the finger is stretched out ($\eta = 0.76$). The tendon has the highest efficiency when the finger is folded ($\eta = 0.83$).

1) Friction model: The results show an improvement of the FTE between the original design and the optimised design of 25%, as can be seen in Appendix A. It is important to note that the practical FTE of these mechanisms can differ from these theoretical results. This is caused by the simplifications we made in the friction model to fit into the scope of this research. Nevertheless, these results prove that this optimisation method results in an improvement of FTE in this model, which will translate when applied to a physical mechanism too. Further development of the friction model is interesting in future research to create more realistic theoretical outcomes. Previous work [1] for instance demonstrates an FTE that is dependent

on the tensile force applied to the tendons.

2) Optimised routing point configuration: The optimisation converges to the routing point configuration in Fig. 5. The outer routing points in this configuration are placed such that the pulleys have the least amount of wrapping angle in the most folded configuration. The middle phalanx also shows the possible redundancy of the third routing point(RP2). These results are partly due to the model incorporating the radii of the routing points.

3) Optimisation over range of configurations: The proposed optimisation method optimises the tendon routing for a certain configuration of the two joint angles. It also enforces continuous contact for the tendon in the extreme positions (fully stretched and fully bent) through a soft constraint. This soft constraint is only active for the fully bent configuration, as in that configuration the wrapping angles are minimal. The method optimises the routing points to have the least amount of wrapping angle at the most bent position while maintaining contact between the tendon and the pulleys. This arises from the fact that in the fully bent configuration the total wrapping angle around the routing points is the dominant source of friction compared to the friction introduced by the pulleys.
Given the constant wrapping angles around the routing points during the full stroke of the finger, it shows that optimising for joint angle extrema encompasses for all joint angle configurations.

4) Optimisation parameters: Currently the optimisation only features the positions of the routing points. Recommended future steps are to look into including other parameters that can have effect on the FTE of the gripper. A parameter such as the radii of the pulleys could be used to find different gripper configurations that live up to the given requirements (range of joint stiffness) where the tendon routing could experience more relaxation.

5) Optimisation method: At last it would be interesting to consider a global optimisation algorithm, as the currently used algorithm could end up with a non-optimal result. A global optimisation algorithm such as the genetic algorithm will, when performed correctly, give a global minimum. This could be interesting to improve the result further in future research.

VI. Conclusion

This paper presents a method to optimise the force transmission efficiency in a tendon-driven mechanism given a predefined tendon route. We have modelled the force transmission efficiency based on the tendon routing, and the dimensions and placement of the routing points and pulleys. With this model we optimised a tendon routing of an existing tendon-driven gripper design to maximise force transmission efficiency while maintaining contact between the tendon and the two pulleys. The results demonstrate an improvement in force transmission efficiency of 25% at the optimised configuration of joint angles while maintaining contact between the tendon and the pulleys over the full stroke.
This improvement can enable more freedom in the design of tendon-driven mechanisms since the losses in force due to friction are decreased. Future work can focus on one of three possible approaches. Firstly is to develop a more accurate friction model to get more accurate results from the optimisation. Secondly is to consider more parameters in the optimisation, such as phalanx lengths and pulley sizes. Finally it is interesting to consider a global optimisation algorithm to ensure that the cost function reaches it's global minimum.

Acknowledgment

I would like to thank dr.ir. W. Roozing and ir. B. Okken for their remarkable guidance during this research. Their critical thinking, experience and attitude have made this bachelor's assignment an absolute pleasure to do.

References

[1] M Bluiminck, "Modelling and control of underactuated finger-based gripper with adjustable compliance for grasping of varying and deformable objects," M.S. thesis, University of Twente, 2022.

[2] L. Marton and B. Lantos, "Modeling, identification, and compensation of stick-slip friction," *IEEE Transactions on Industrial Electronics*, vol. 54, no. 1, pp. 511–521, 2007.

[3] H. Dong, E. Asadi, C. Qiu, J. Dai, and I.-M. Chen, "Geometric design optimization of an under-actuated tendon-driven robotic gripper," *Robotics and Computer-Integrated Manufacturing*, vol. 50, pp. 80–89, 2018.

[4] Y. Peng, Y. Wei, and M. Zhou, "Efficient modeling of cable-pulley system with friction based on arbitrary-lagrangian-eulerian approach," *Applied Mathematics and Mechanics*, vol. 38, no. 12, pp. 1785–1802, 2017.

[5] *Spiderwire dura4 braid yellow 300m*, https : / / www . sportvisgigant . nl / spiderwire - dura4 - braid - yellow - 300m - 010mm-86872967.html, Accessed: 2024-01-27.

[6] *Coefficient of friction reference chart*, https://www.schneider-company . com / coefficient - of - friction - reference - chart/, Accessed: 2024-01-27.

[7] *Iglide® plastic bushings - coefficients of friction*, https : / / www.igus . com / info / plain - bearings - iglide - plastic - bushings - coefficients-of-friction-ca, Accessed: 2024-01-27.

APPENDIX

A: DESIGN PARAMETERS CURRENT DESIGN [1]

Parameter		**Value**	**Units**
Width phalanges and base	W	10	mm
Pulley radii	r_{P1}, r_{P2}	7.5	mm
Routing point radii	$r_{RP0}, r_{RP1}, r_{RP2}, r_{RP3}$	1.5	mm
Length base	L_0	40	mm
Length phalanges	L_1, L_2	47.5	mm
Center $P1$ (w.r.t. frame B)	(x_{P1B}, y_{P1B})	(0,0)	mm
Center $P2$ (w.r.t. frame C)	(x_{P2C}, y_{P2C})	(0,0)	mm
Center $RP0$ (w.r.t. frame A)	(x_{RP0A}, y_{RP0A})	(-13.90,-10)	mm
Center $RP1$ (w.r.t. frame B)	(x_{RP1B}, y_{RP1B})	(-4.80,20.66)	mm
Center $RP2$ (w.r.t. frame B)	(x_{RP2B}, y_{RP2B})	(-4.80,35.98)	mm
Center $RP3$ (w.r.t. frame C)	(x_{RP3C}, y_{RP3C})	(-6.30,13.40)	mm
Joint 1 range (w.r.t. frame A)	Range(θ_1)	[0.5π,0]	rad
Joint 2 range (w.r.t. frame B)	Range(θ_2)	[0,0.5π]	rad

B: THE ROUTING POINT COORDINATES FOR THE INITIAL CONFIGURATION AND THE OPTIMISED CONFIGURATION

Parameter	**Value (x, y)**	**Unit**
I.C. $RP0$ w.r.t. frame A	(-13.90, -10.00)	mm
Optimised center $RP0$ w.r.t. frame A	(-10.99, -10.00)	mm
I.C. $RP1$ w.r.t. frame B	(-4.80, 20.66)	mm
Optimised center $RP1$ w.r.t. frame B	(4.75, 16.50)	mm
I.C. $RP2$ w.r.t. frame B	(-4.80, 35.98)	mm
Optimised center $RP2$ w.r.t. frame B	(5.97, 25.27)	mm
I.C. $RP3$ w.r.t. frame C	(-6.30, 13.40)	mm
Optimised center $RP3$ w.r.t. frame C	(-5.61, 9.01)	mm